

# Hydrodynamic oscillations and tunable swimming speed in squirmers close to repulsive walls

Juho S. Lintuvuori<sup>1</sup>, Aidan T. Brown<sup>2</sup>, Kevin Stratford<sup>3</sup> and Davide Marenduzzo<sup>2</sup>

<sup>1</sup> *Laboratoire de Physique des Solides, Université Paris-Sud, UMR 8502 - 91405, Orsay, France*

<sup>2</sup> *SUPA, School of Physics and Astronomy, University of Edinburgh, UK.*

<sup>3</sup> *EPCC, School of Physics and Astronomy, University of Edinburgh, UK.*

We present a lattice Boltzmann study of the hydrodynamics of a fully resolved squirmer, radius  $R$ , confined in a slab of fluid between two no-slip walls. We show that the coupling between hydrodynamics and short-range repulsive interactions between the swimmer and the surface can lead to hydrodynamic trapping of both pushers and pullers at the wall, and to hydrodynamic oscillations in the case of a pusher. We further show that a pusher moves significantly faster when close to a surface than in the bulk, whereas a puller undergoes a transition between fast motion and a dynamical standstill according to the range of the repulsive interaction. Our results critically require near-field hydrodynamics; they further suggest that it should be possible to control density and speed of squirmers at a surface by tuning the range of steric and electrostatic swimmer-wall interactions.

PACS numbers: 47.63.mf, 87.17.Jj, 47.63.Gd

*Introduction:* Motile organisms such as bacteria and sperm cells have a natural tendency to be attracted towards surfaces, and to swim near them [1]. This phenomenon may be relevant for the initial stage of the formation of biofilms, the microbial aggregates which often form over surfaces in nature. On the other hand, experiments have shown that this tendency is not unique to living swimmers, and is exhibited by phoretic active particles as well [2–4]: in that context, it has been exploited for example, to attract microswimmers inside a colloidal crystal, where they exhibit stochastic orbiting around the colloids [4]. The interaction between self-propelled particles and walls also provides a microscopic basis for the rectification of bacterial motion by asymmetric geometries (*e.g.* funnels) [5].

Previous work has proposed two possible mechanisms for surface accumulation of self-motile particles. A first view is that they do so through far-field hydrodynamic interactions [6]. Another possibility is that motility itself, in the absence of solvent-mediated interactions, leads to accumulation [7, 8]: this mechanism requires a small enough channel, where the gap size is of the order of the typical distance travelled ballistically by the active particles, before rotational diffusion or tumbling reorients them. The case of phoretic particles may be more complex [4, 9], and may depend on the dynamics of the chemicals reacting at the swimmers surface. Schaar *et al.* recently showed that hydrodynamic torques strongly affect the “detention times” over which microswimmers reside near no-slip walls [10]. The behaviour is partly controlled by the details of the force distribution with which active particles stir the surrounding fluid; previous work has also shown that these determine the equilibria of a spherical squirmer near a flat surface [11, 12].

Previous theories have not systematically studied the effects of a short range repulsion between the particle

and the wall; in practice this is always present in experiments, either due to screened electrostatics, for charged walls, or due to steric interactions, *e.g.* for polymer-coated surfaces. Here we show that explicitly including this repulsion is important, and strongly affects the dynamics near a surface. The interplay between hydrodynamics and short range repulsion can lead to trapping, periodic swimming, and to a swimming speed which can be significantly different than in the bulk. These results provide an experimentally viable route to tune the microswimmer concentration and speed near a no-slip surface. Our finding of oscillatory near-wall dynamics also provides a possible explanation why swimmers exerting extensile forces on the fluid (pushers) are routinely observed to accumulate at walls experimentally (*e.g.* bacteria), whereas recent theoretical calculations [11] predict that the equations of motion do not possess any stationary bound state solution (*i.e.* where the particle swims stably along the wall in steady state). These results are compatible if the steady state is an oscillatory instead of stationary, as our simulations suggest is the case.

*Squirmer model:* A popular model for swimmer hydrodynamics is a spherical squirmer – a particle which is rendered self-motile through a surface slip velocity [13]. To study the dynamics of a model squirmer in confinement we employ a lattice Boltzmann (LB) method [14]. The tangential (slip) velocity profile at the particle surface leading to the squirmer motions is given by [13]

$$u(\phi) = 2 \sum_{n=1}^{\infty} \frac{\sin \phi}{n(n+1)} \frac{dP_n(\cos \phi)}{d \cos \phi} B_n \quad (1)$$

where  $\phi$  is the polar angle and  $P_n$  is the  $n$ th Legendre polynomial [11].

In the LB method a no-slip boundary condition at the fluid/solid interface can be achieved by using a standard method of bounce-back on links (BBL) [15, 16]. When

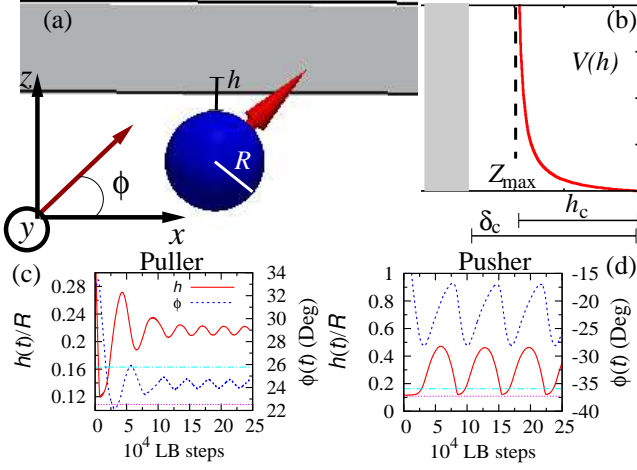


FIG. 1. (a) A cartoon showing an example of a squirmer near a flat wall, defining the gap size  $h$  and angle  $\phi$  used in the text. (b) There is a repulsive interaction between the wall and a squirmer. Examples of steady state  $\phi(t)$  and  $h(t)$  observed for (c) puller and (d) pusher dynamics near a flat wall in the absence of thermal noise are also shown. The interaction range is  $\delta_c \sim 0.16R$  (dot-dashed line) and the potential diverges at  $\sim 0.11R$  (dotted line).

the boundary is moving (e.g. colloidal particle) the BBL condition needs to be modified to take into account particle motion [17]. These local rules can include additional terms, such as surface slip velocity (Eq. 1): in this way it is possible to simulate squirming motion [18, 19]. Our implementation also includes the effects of thermal noise [20], thus allowing simulations to be carried out using a finite Péclet number.

*Simulation parameters:* We limit our simulations to simple squirmers with  $B_n = 0, n \geq 3$ , but consider both pushers ( $B_2 < 0$ ) and pullers ( $B_2 > 0$ ). The chosen simulation parameters in lattice units (LU) are:  $B_1 = 0.0015$ ,  $B_2 = \pm 0.0075$ , (which gives a swimming velocity in the bulk equal to  $u_0 = \frac{2}{3}B_1 = 10^{-3}$ LU and  $\beta \equiv \frac{B_2}{B_1} = \pm 5$ ), fluid viscosity  $\eta = 0.1$  and thermal noise  $k_B T = 10^{-5}$  in lattice units (LU). We considered a fully resolved swimmer with radius  $R = 9.2$ LU (Fig. 1(a)) [21]. The physics is governed by two main hydrodynamic dimensionless quantities: the Reynolds and Péclet numbers. Using the parameters above, these are  $Re = \frac{u_0 R}{\eta} \approx 0.09$  and  $Pe = \frac{u_0}{D_r R} \approx 2 \times 10^4$  respectively, where  $D_r = \frac{k_B T}{8\pi\eta R^3}$ , is the rotational diffusion constant. Our simulations were carried out in a rectangular simulation box  $120 \times 120 \times 96$ , with periodic boundary conditions in  $X$  and  $Y$  and solid walls at  $Z_{\text{bottom}} = 1$  and  $Z_{\text{top}} = 96$ .

In order to achieve a well defined repulsive interaction range  $\delta_c$ , we employ the following potential between the particle and the wall,

$$V(h) = \epsilon (\sigma/h)^\nu. \quad (2)$$

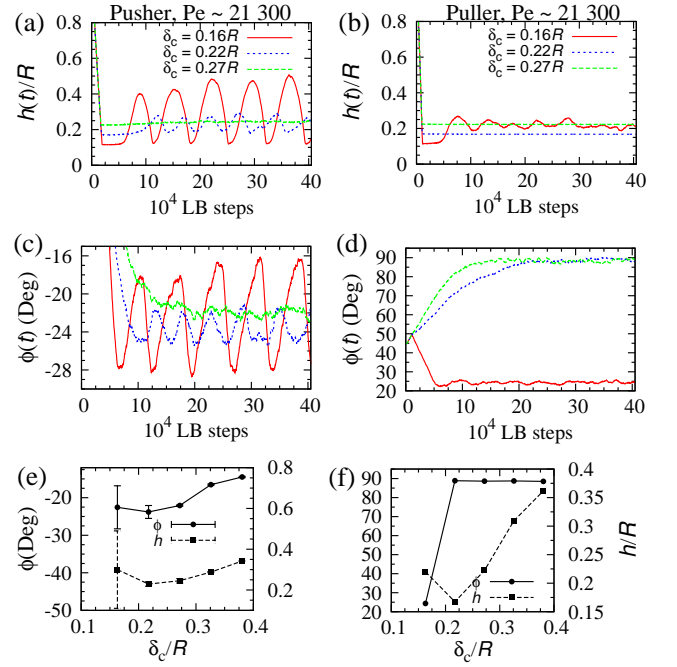


FIG. 2. Simulation results when the range of the soft repulsion is varied  $\delta_c \approx 0.16R$  (solid line),  $\delta_c \approx 0.22R$  (short dashes) and  $\delta_c \approx 0.27R$  (dashed line), with  $Pe \approx 2 \times 10^4$ . Time developments of  $h(t)/R$  (a) for a pusher and (b) for a puller as well as  $\phi(t)$  for (c) a pusher and (d) a puller. (Note the sudden change in behaviour for puller is further discussed in the text). The steady state  $h$  and  $\phi$  as a function of  $\delta_c$  for (e) pusher (the errorbars give the amplitude of the oscillations) and (f) puller. (Initial conditions:  $h_0 \approx 1.1R$  and  $\phi_0 = 45.0^\circ$ ;  $Pe \approx 2 \times 10^4$ ).

The potential depends on the surface-to-surface separation  $h$  and is cut-and-shifted,

$$h = Z_{\text{max}}^{\text{min}} \pm r(z) - R, \quad (3)$$

$$V_{cs}(h) = V(h) - V(h_c) - (h - h_c) \left. \frac{\partial V(h)}{\partial h} \right|_{h=h_c}, \quad (4)$$

to ensure that the potential and force goes smoothly to zero at  $h = h_c$ . Parameters were chosen as,  $\epsilon = 0.004$ ,  $\sigma = 0.1$ ,  $\nu = 1.0$ . By choosing  $Z_{\text{max}} = Z_{\text{top}} - (\delta_c - h_c)$  ( $Z_{\text{min}} = Z_{\text{bottom}} + (\delta_c - h_c)$ ) and keeping  $h_c = 0.5$ LU constant, we can have a well defined repulsion range  $\delta_c$ , while keeping  $h_c$  and thus the potential form constant (Fig. 1(b)). For the calculation of the gap size between the squirmer and the solid surface  $h$  (Fig. 1(a)), we define the wall location half-way between the solid node and first fluid node ( $Z_{\text{bottom}} = 1.5$  and  $Z_{\text{top}} = 95.5$ ), as customary in LB simulations.

*Results:* In Fig. 1(c,d) we plot the evolution of the gap size  $h(t)/R$  and of the angle  $\phi$  between the squirmer direction and the surface plane (Fig. 1(a)). For a puller, after an initial collision with the soft repulsive wall, the hydrodynamically induced torques rotate the particle so that it settles to swim parallel to the no-slip wall (be-

yond the excluded volume interaction range; dot-dashed line in Fig. 1(c)) with a distance  $h \sim 0.2R$ , in very good agreement with theoretical predictions [11]. In steady state the puller points towards the surface,  $\phi \sim 24$  degrees (Fig. 1(c)). For a  $\beta = -5$  pusher, previous theories based only on hydrodynamic interactions predict no stable swimming near surface [11]; however in experiments, bacterial swimmers (which are pushers), or phoretic swimmers which are thought to be pushers, are typically observed to accumulate and undergo stable swimming at no-slip surfaces [2, 4, 6]. Strikingly, our simulations (Fig. 1(d)), show a periodic orbit both in  $h(t)$  and  $\phi(t)$ , of a pusher near the confining surface. During a collision with the soft-repulsive wall, hydrodynamic torques reorient the particle (Fig. 1(d)) leading to swimming away from the wall ( $\phi$  is on average  $< 0$  in Fig. 1(d)). This much is expected; surprisingly, however, the long range hydrodynamic interactions between the swimmer and the wall, lead to another reorientation of the swimmer so that it starts to swim towards the wall again. The cycle repeats leading to the hydrodynamic oscillations near the no-slip surface (Fig. 1(d)), while  $\phi(t) < 0$  during the oscillations, significant part of the trajectory  $h(t)$  is spend beyond the external repulsion range (dot-dashed line in Fig. 1(d)). Interestingly, for both pusher and puller dynamics, the hydrodynamically induced attraction is strong enough to resist the effects of thermal noise (see Fig. 2(a,b)).

The external soft repulsion, and in particular its range, plays a key role in determining the swimming dynamics. This can be seen from  $\phi(t)$  and  $h(t)$  results presented in Fig. 2(a-d), for different repulsive ranges ( $\delta_c = 0.16R$ ,  $0.22R$  and  $0.27R$ ): these simulations include the effect of thermal noise, with  $Pe \approx 2 \times 10^4$ , and were all initialised with the particle initially sitting at  $h_0 \approx 1.1R$  with initial angle  $\phi_0 = 45^\circ$ . For all ranges considered, both the pusher and the puller are found to be swimming near the surface (Fig. 2(a,b)). However, the hydrodynamic oscillations in the pusher dynamics (visible both in  $h(t)$  and  $\phi(t)$  Fig. 2(a,c)) are suppressed when the repulsive range is increased, and disappear altogether for  $\delta_c = 0.27R$  (Fig. 2). In this case, both pusher and puller lean onto the soft repulsive wall (*i.e* in steady state  $h < \delta_c$ ) with  $h$  increasing with  $\delta_c$ , (Fig. 2(e,f)). The plot of the swimming orientation  $\phi(t)$  (Fig. 2(c,d)) confirms the absence of oscillations: the pusher swims with keeping a stable orientation tilted away from the wall, with  $\phi$  slightly decreasing when  $\delta_c$  is increased (Fig. 2(e)); the puller instead is rotated by hydrodynamic torques to point towards the wall, so that  $\phi \sim 90^\circ$  (this is actually always the case as soon as  $\delta_c \geq 0.22R$  (Fig. 2(f))).

Most existing theories of swimmer hydrodynamics rely on the far-field approximation which is based on the velocity field a swimmer generates at distances which are large with respect to its size. The far-field approximation can be adapted to include a no-slip wall [22]: as a

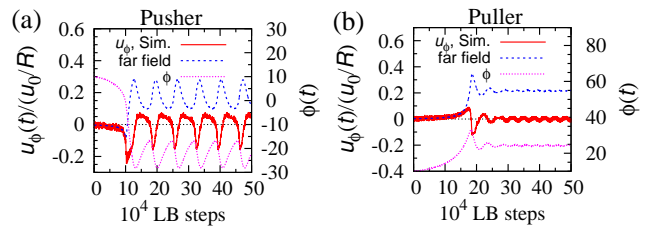


FIG. 3. Observed simulation and far field results for  $u_\phi(t)/(u_0/R)$  for (a) pusher and (b) puller. The repulsive range was  $\delta_c \approx 0.16R$  (initial conditions  $h_0 \approx 3.25R$  and  $\phi_0 = 10^\circ$ ; no thermal noise).

result one obtains the following expressions for the time derivative of  $\phi$ ,  $x$  and  $z$  at a given time,

$$\begin{aligned} \frac{d\phi}{dt} &= \frac{u_0}{R} \left[ -\frac{9\beta \sin(2\phi)}{64} \left(\frac{R}{h'}\right)^3 + \frac{3 \cos \phi}{16} \left(\frac{R}{h'}\right)^4 \right] \\ \frac{dx}{dt} &= u_0 \left[ \cos \phi + \frac{9\beta \sin(2\phi)}{32} \left(\frac{R}{h'}\right)^2 - \frac{\cos \phi}{8} \left(\frac{R}{h'}\right)^3 \right] \\ \frac{dz}{dt} &= u_0 \left[ -\sin \phi + \frac{9\beta (1 - 3 \sin^2 \phi)}{32} \left(\frac{R}{h'}\right)^2 + \frac{\sin \phi}{2} \left(\frac{R}{h'}\right)^3 \right], \end{aligned} \quad (5)$$

where  $\beta = \frac{B_2}{B_1}$  and  $h'$  is the distance from the centre of the particle to the confining wall ( $h' \rightarrow h + R$  in Fig. 1(a)). To allow detailed comparison between our model and the far field approximations, we carried out simulations starting with  $h_0 \approx 3.25R$  and  $\phi_0 = 10^\circ$  and at each point we calculated the expression for  $d\phi/dt$ ,  $dx/dt$  and  $dz/dt$  either directly from our numerics, or by substituting the instantaneous values of  $h(t)$  and  $\phi(t)$  into Eqs. 5, which provides the far-field estimate of the system evolution given its current state.

First, we discuss the results for the angular velocity,  $d\phi/dt$  (Fig. 3). For early times, there is good agreement between the rotational dynamics predicted by the far-field approximation and that found in our direct numerical simulations: we observe a decrease (pusher) and increase (puller) of  $\phi(t)$  from the initial  $\phi_0 = 10^\circ$ . Later on the far-field estimate no longer captures the dynamics observed in simulation. In steady state the far field predicts  $\frac{d\phi}{dt} > 0$  while simulations show no net motion of  $\phi(t)$ , as shown in Fig. 2(c,d). This suggests that near-field hydrodynamics is crucial in determining the trapping of the puller and the oscillations of the pusher. The dynamics of  $z$ , determining approach to the surface, leads to the same conclusion: prior to interacting with the repulsive wall, the far-field works well, when the repulsive interaction is reached, there is a notable disagreement (see Suppl. Fig. S1); this persists after correcting the far-field prediction to include the repulsive interaction, with an extra normal velocity  $u_w = -\frac{1}{\gamma} \frac{\partial V(h)}{\partial h}$  (where  $\gamma = 6\pi\eta R$ ). The dominance of the near-field is confirmed by noting that our observed steady state ( $h$ ,  $\phi$ ) for a *puller* (Fig. 1(c) and

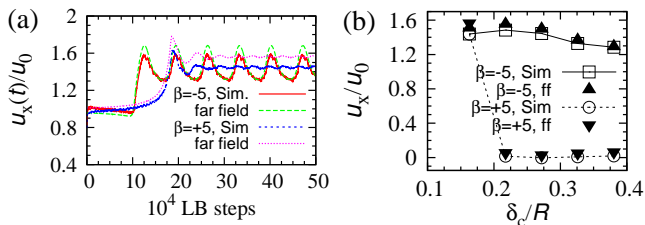


FIG. 4. (a) Simulations and far field results for  $u_x(t)/u_0$  for pusher ( $\beta = -5$ ) and puller ( $\beta = +5$ ) as well as  $\phi(t)$  for a puller ( $\beta = +5$ ), when the repulsion range was  $\delta_c \approx 0.22R$  (initial conditions  $h_0 \approx 3.25R$ ,  $\phi_0 = 10^\circ$ ; no thermal noise). (b) The steady state  $u_x/u_0$  as a function of the repulsion range  $\delta_c$ , from simulations and far field calculations (initial conditions:  $h_0 \approx 1.1R$ ,  $\phi_0 = 45^\circ$ ;  $Pe \approx 2 \times 10^4$ ).

Fig. 2(d)) is in agreement with theoretical calculations taking into account near and far-field hydrodynamics but ignoring short range repulsions [11].

For the movement along the wall ( $dx/dt \equiv u_x$  in Eq. 5), the situation is markedly different. Now simulations and far field predictions agree well at all times (Fig. 4(a); similar conclusions were reached by Spagnolie and Lauga who studied the dynamics of a swimmer before collisions with the wall [22]). Far away from the wall,  $u_x \sim u_0$  (the swim speed in the bulk) as expected. Upon first approaching the wall, the pusher shows a slight decrease in  $u_x$  – we attribute this to the rotational drag encountered when going from the initial  $\phi_0 = 10^\circ$  to the steady state value  $\phi(t) \sim -25^\circ$  (Fig. 4(a)). Instead, the puller shows a slight increase in  $u_x$ , while smoothly rotating its director towards the wall normal (see Fig. 3(b)).

Remarkably, the steady state velocities for both swimmers are considerably larger than in the bulk, i.e. the presence of a surface accelerates the motion ( $\sim 50\%$  faster than in the bulk, see Fig. 4(a)). The increase in the swimming speed near a solid surface can be understood intuitively by considering the swimming mechanism. The pusher is propelled from behind, thus when it is pointing away from the surface is pushing the fluid flow against a solid wall – this should enhance the swim speed, as predicted for swimmers in porous media [4, 23]. Interestingly the speed increase is retained also for the periodic swimming. The speed up of the puller can be understood in a similar way, as the squirmer is now oriented towards the wall so effectively grabs the no-slip wall and can gain momentum from this. Although our speed increase occurs close to a solid wall, it is interesting to note that very recent experiments reported an enhanced swimming speed up to  $\sim 2u_0$  for Janus colloids on a water-air interface [24].

Increasing the range of the repulsive interaction leaves the pusher dynamics along the surface mostly unaffected: we find that  $u_x > u_0$  for all the interaction ranges considered, as shown in Fig. 4(a,b). The case of the puller

is very different, as any repulsive interaction extending past the equilibrium swimming distance  $\sim 0.2R$  leads to hydrodynamic torques orienting the particle towards the wall (Fig. 2(d)); see also Suppl. Fig. S2, which shows that the far-field approximation for the tangential speed remains good in this case as well). The reorientation occurs independently of initial conditions (in Fig. 4(b) the initial angle is almost tangential,  $\phi_0 = 10^\circ$ ), and leads to a dramatic slowing down of the particle, whose motion virtually comes to a standstill when  $\delta_c \geq 0.22R$  (see Fig. 4(b)).

In all the cases we have considered, the rotational motion has a fundamental role on the dynamics of the particle, and this is affected by  $\delta_c$ . It should be noted that the soft repulsion only *slows down* the particle movement along the the surface normal (as visible from Suppl. Fig. S1 for  $dz/dt$ ), and it *does not* create any torques; therefore any rotational motion of the particle only arises from the combination of hydrodynamic and Brownian forces, which can act differently due to the repulsive wall because they have more or less time to set in. In other words, the repulsive interaction with the walls controls the relative timescales of translational approach and rotation due to hydrodynamic torques, leading to the observed phenomena.

*Conclusions:* We have presented a study of fully resolved spherical squirmers swimming between two solid walls, using a microscopic model which prescribes a slip velocity at the particle surface. Our results show that the repulsive interaction, which was neglected routinely in previous theories of swimmers interacting with a surface, plays a very important role in the squirmer’s dynamics. First, it can stabilise hydrodynamic oscillations of a pusher close to the wall. This result can clarify some important aspects of the hydrodynamics of pushers close to a wall. While experiments routinely observe that bacteria (which are known to be pushers) or phoretic swimmers (which are thought to be pushers) are attracted to and swim near flat surfaces [2, 6], a recent systematic investigation has demonstrated that in the parameter range we consider ( $\beta \sim -5$ ) there is no stable bound state with the pusher swimming near the wall [11]. One way to reconcile these results is if the trajectory of the swimmer at late times is oscillatory (a limit cycle in the  $(h, \phi)$  plane) instead of having constant velocity (a stationary point in the  $(h, \phi)$  plane). Second, we find that the swim velocity of a pusher is significantly increased with respect to the bulk limit: this behaviour can be understood as the particle, on average, is directed away from the wall and pushes on it, hence enhancing its speed. Third, we find that the tangential velocity of a puller changes dramatically with the range of the repulsive interaction with the wall: if this range is small, the speed increases, and is comparable to that of a pusher; if the range exceeds a critical threshold, the thermodynamic slowdown close to the wall combines with hydrodynamic torques to rotate

the puller, so that it collides with the surface head on and stops moving. Our results require near-field hydrodynamics, as the far-field approximation poorly captures the rotational dynamics we observe.

Our results further imply that the existence and extent of steric or electrostatic repulsion of the wall could be tuned to control properties such as the number density and swim speed of active particles near a surface. Experimentally this could be achieved, by varying either the buffer concentration (for electrostatic repulsion) or the polymer coverage of the surface (for steric repulsion). These predictions should be testable with experiments using bacterial swimmers or artificial microswimmers, although phoretic particles may not be ideally suited for these tests, in view of the importance of chemical gradients and chemical dynamics for their physics [4, 9, 25–27], here neglected.

*Acknowledgements:* This work was funded by EU intra-European fellowship 623637 DyCoCoS FP7-PEOPLE-2013-IEF and UK EPSRC grant EP/J007404/1.

- 
- [1] Lord Rothschild, *Nature* **198**, 1221 (1963).  
 [2] A. T. Brown and W. C. K. Poon, *Soft Matter* **10**, 4016 (2014).  
 [3] D. Takagi, J. Palacci, A. B. Braunschweig, M. J. Shelley, and J. Zhang, *Soft Matter* **10**, 1784 (2014).  
 [4] A. T. Brown, *Soft Matter*, Submitted, arXiv:1411.6847 (2015).  
 [5] P. Galadja, J. Keymer, P. Chaikin, and R. Austin, *J. Bacteriol.* **189**, 8704 (2007).  
 [6] A. P. Berke, L. Turner, H. C. Berg, and E. Lauga, *Phys Rev Lett* **101**, 038102 (2008).  
 [7] G. Li and J. X. Tang, *Phys Rev Lett* **103**, 78101 (2009).  
 [8] J. Elgeti and G. Gompper, *EPL* **101**, 48003 (2013).  
 [9] W. E. Uspal, M. N. Popescu, S. Dietrich, and M. Tassinkevych, *Soft Matter* **11**, 434 (2015).  
 [10] K. Schaar, A. Zöttl, and H. Stark, *Phys. Rev. Lett.* **115**, 038101 (2015).  
 [11] K. Ishimoto and E. A. Gaffney, *Physical Review E* **88**, 062702 (2013).  
 [12] G.-J. Li and A. M. Ardekani, *Phys. Rev. E* **90**, 013010 (2014).  
 [13] M. J. Lighthill, *Communications on Pure and Applied Mathematics* **5**, 109 (1952).  
 [14] M. E. Cates, K. Stratford, R. Adhikari, P. Stansell, J.-C. Desplat, I. Pagonabarraga, and A. J. Wagner, *J. Phys. Condens. Mater.* **16**, S3903 (2004).  
 [15] A. J. C. Ladd, *J. Fluid Mech.* **271**, 285 (1994).  
 [16] A. J. C. Ladd, *J. Fluid Mech.* **271**, 311 (1994).  
 [17] N.-Q. Nguyen and A. J. C. Ladd, *Phys. Rev. E* **66**, 046708 (2002).  
 [18] I. Llopis and I. Pagonabarraga, *J. Non-Newtonian Fluid Mech.* **165**, 946 (2010).  
 [19] I. Pagonabarraga and I. Llopis, *Soft Matter* **9**, 7174 (2013).  
 [20] R. Adhikari, K. Stratford, M. E. Cates, and A. J. Wagner, *Europhys. Lett.* **71**, 473 (2005).  
 [21] Assuming a particle radius  $10\mu\text{m}$  and using the kinematic viscosity of water  $10^{-6}\frac{\text{m}^2}{\text{s}}$  a single simulation length and time unit can be mapped to  $\sim 1\mu\text{m}$  and  $0.1\mu\text{s}$ , giving a swimming speed  $u_0 = 10\frac{\text{mm}}{\text{s}}$ . The distance between the two walls is  $\sim 100\mu\text{m}$ , which corresponds to typical experiments [6].  
 [22] S. E. Spagnolie and E. Lauga, *J. Fluid Mech.* **700**, 105 (2012).  
 [23] R. Ledesma-Aguilar and J. M. Yeomans, *Phys. Rev. Lett.* **111**, 138101 (2013).  
 [24] X. Wand, M. In, C. Blanc, M. Nobili, and A. Stocco, *Soft Matter* (2015), DOI: 10.1039/C5SM01111F.  
 [25] I. Theurkauff, C. Cottin-Bizonne, J. Palacci, C. Ybert, and L. Bocquet, *Phys. Rev. Lett.* **108**, 268303 (2012).  
 [26] T. Bickel, A. Majee, and A. Würger, *Physical Review E* **88**, 012301 (2013).  
 [27] F. Ginot, I. Theurkauff, D. Levis, C. Ybert, L. Bocquet, L. Berthier, and C. Cottin-Bizonne, *Phys. Rev. X* **5**, 011004 (2015).

## Supplementary information for: Hydrodynamic oscillations and tunable swimming speed in squirmers close to repulsive walls

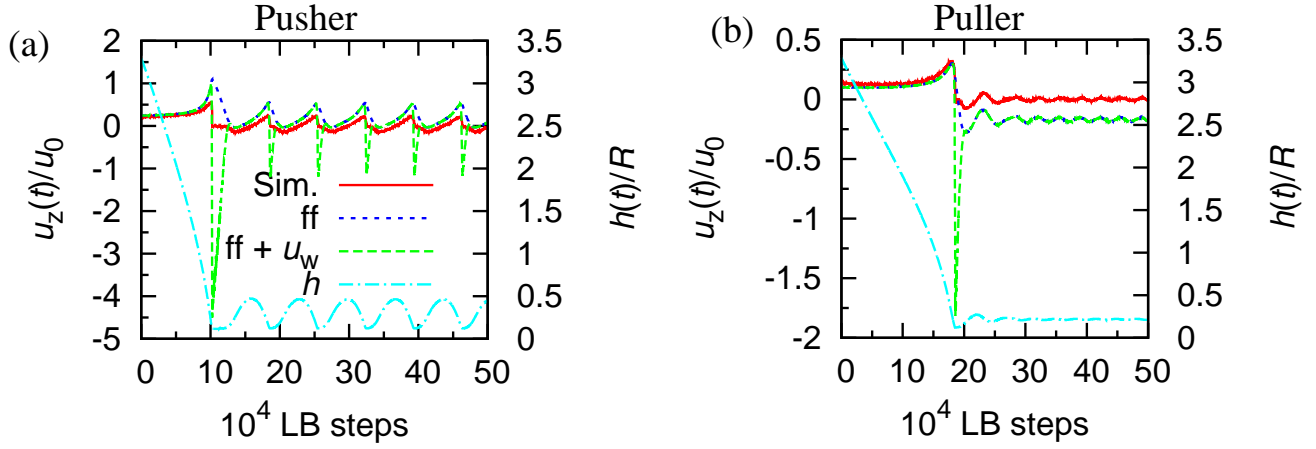


FIG. S1. Observed simulation results and far field results for  $u_z(t)/u_0$  for (a) pusher and (b) puller. The repulsion range was  $\delta_c \approx 0.16R$  (initial conditions  $h_0 \approx 3.25R$  and  $\phi_0 = 10^\circ$ ; no thermal noise)

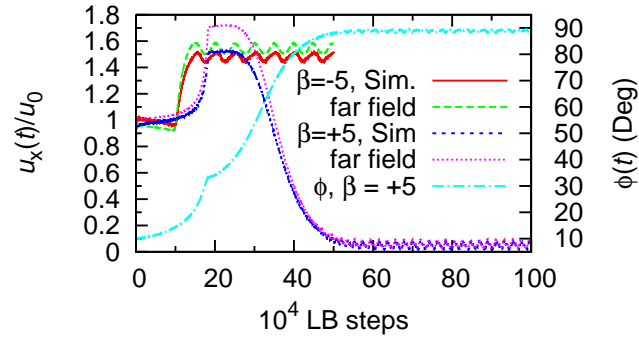


FIG. S2. Simulations and far field results for  $u_x(t)/u_0$  for pusher ( $\beta = -5$ ) and puller ( $\beta = +5$ ) as well as  $\phi(t)$  for a puller ( $\beta = +5$ ), when the repulsion range was  $\delta_c \approx 0.22R$  (initial conditions  $h_0 \approx 3.25R$ ,  $\phi_0 = 10^\circ$ ; no thermal noise).